# Chance-Constrained Energy Management System for Power Grids With High Proliferation of Renewables and Electric Vehicles

Bo Wang , *Student Member, IEEE*, Payman Dehghanian , *Member, IEEE*, and Dongbo Zhao , *Senior Member, IEEE*

*Abstract*—This paper proposes a two-stage energy management system (EMS) for power grids with massive integration of electric vehicles (EVs) and renewable energy resources. The first stage economic dispatch determines the optimal operating points of charging stations and battery swapping stations (BSS) for EVs under plug-in and battery swapping modes, respectively. The proposed stochastic model predictive control (SMPC) problem in this stage is characterized through a chance-constrained optimization formulation that can effectively capture the system and the forecast uncertainties. A distributed algorithm, the alternating direction method of multipliers (ADMM), is applied to accelerate the optimization computation through parallel computing. The second stage is aimed in coordinating the EV charging mechanisms to continuously follow the first-stage solutions, i.e., the target operating points, and meeting the EV customers' charging demands captured via the Advanced Metering Infrastructure (AMI). The proposed solution offers a holistic control strategy for large-scale centralized power grids in which the aggregated individual parameters are predictable and the system dynamics do not vary sharply within a short time-interval.

*Index Terms*—Economic dispatch, electric vehicle (EV), energy management system (EMS), chance-constrained optimization, stochastic model predictive control (SMPC).

## Nomenclature

### *Indices*

| | |
|---|---|
| $i$ | Index for state variables $(1, \ldots, n)$. |
| $j$ | Index for EV numbers. |
| $m$ | Index for stochastic scenarios $(1, \ldots, M)$. |
| $k$ | Index for time-steps $(1, \ldots, K)$. |
| $s$ | Index for EV groups $(1, \ldots, S)$. |
| $t$ | Index for time. |

### *Parameters and Variables*

| | |
|---|---|
| $\alpha$ | Auxiliary variable for convex approximation. |

| | |
|---|---|
| $\alpha_c, \alpha_d$ | Charge/discharge efficiency of the battery. |
| $\epsilon$ | Probability of constraint violation. |
| $\gamma$ | Penalty factor. |
| $\lambda$ | Scaled dual variable in ADMM. |
| $\Delta t$ | Length of the time-step. |
| $\Delta P_{G,i}$ | Ramp rate of the generating unit $i$. |
| $B_s$ | SOC of battery swapping station. |
| $c_d$ | Battery degradation cost per MWh. |
| $C_i(P_{G,i})$ | Operating cost function of generating unit $i$. |
| $E_C$ | Forecasted energy consumption of plug-in EVs in the next 24 hours. |
| $E_{dep}$ | EV's energy demand upon departure. |
| $E_p$ | Energy state of the plug-in EVs. |
| $E_{ini}$ | Energy state of the plug-in EVs at the initial time interval. |
| $k_1, k_2$ | Current and departure time intervals for EVs under plug-in mode. |
| $L_1, L_2$ | Look-ahead time windows for SED and OPF, respectively. |
| $L_c$ | Total energy allocated to plug-in EVs. |
| $P_G$ | Active power of generating units. |
| $P_{net}$ | The net generation of buses. |
| $t_{dep}$ | EV departure time. |
| $TU$ | Auxiliary variable. |
| $u$ | System control variable. |
| $u_c$ | Converted power to stored energy. |
| $u_d$ | Converted power from BSS to electricity. |
| $u_l$ | Allocated power for plug-in EVs sent from the ISO to a specific utility. |
| $u_l^{min}, u_l^{max}$ | Minimum and maximum charging capacity of plug-in EVs. |
| $u_p$ | Power allocated to plug-in EVs. |
| $u_s$ | Energy consumption of EVs by swapping the batteries. |
| $w$ | System disturbance. |
| $x$ | System state variable. |
| $z$ | Common global variable in ADMM. |

## I. Introduction

**D**EMAND side management (DSM) has been employed as an effective mechanism by the utility operators to mitigate the system operating costs at the peak load intervals while best meeting the carbon emission targets [1]. In contrast with

those DSM programs that primarily operate through mutual interactions with the customers (by sending them the energy price signals and seeking their response accordingly), direct load control (DLC) mechanisms allow the utility to switch on and off the end-use devices when certain system operating conditions unfold. In so doing, many electric utilities have leveraged the advanced metering infrastructure (AMI) for DLC communications [2]. With the wide deployment of the AMI in practice, real time measurement and control of the emerging flexible loads, e.g., electric vehicles (EVs), becomes viable system-wide [3]. This in turn calls for well-designed control and scheduling mechanisms allowing the operator to harness the large-scale EV demand flexibility.

In recent years, optimal charging management and scheduling of EVs under both plug-in and battery swapping modes have been extensively explored in the literature. Both globally and locally optimal charging and discharging schedules are suggested in [4] for EVs under plug-in operating mode. Many literature propose locally optimal charging and discharging schedules to maximize the benefits of particular stakeholders. A cyber-physical energy management system for networked nanogrids with battery swapping stations (BSSs) is introduced in [5]. Optimal day-ahead operation and service scheduling of the BSS is investigated in [6]. Pricing signals are widely utilized in decentralized charging strategies to coordinate the aggregators and avoid the locally optimal solutions. Scheduling of the plug-in EVs with co-optimized customer and system objectives is addressed in [7] where the battery degradation, customer costs, and system load profiles are taken into account. However, the scheduling scheme presented in [7] is centered on the electricity market price, the real-time dynamics of which are prominently affected by the high penetration of EVs. In response, dynamic pricing scheme and optimal charging scheduling of the BSS is studied in [8]. Efforts have also been made in [9] to structure a dynamic charging mechanism that is able to adjust and update the EV charging prices according to the tracked demand portfolios. The proposed method in [9] is to incentivize the customers to meet the charging station demand requirements, which may not be an effective assumption in practice considering the random behaviours of EV customers.

New energy management systems (EMSs) are needed to effectively capture the system uncertainties and respond to the growing demand for additional grid-scale flexibility, especially with the emerging trends in high proliferation (rapid increase) of renewables and EVs in the near future. Economic dispatch in power grids with high penetration of renewables and energy storage systems is studied in [10], [11], where stochastic models are developed based on model predictive control (MPC) to minimize the system operating cost over different scenarios that best reflect the uncertainty of future model parameters. In [12], a chance-constrained formulation is suggested for optimal power flow (OPF) in radial distribution systems with stochastic distributions of renewable forecasts. The chance constraints of the stochastic MPC (SMPC) offers a holistic approach that systematically seeks a trade-off between the control objectives and probabilistic uncertainty constraints [13]. A two-stage decision support tool for isolated microgrids with

energy storage is proposed in [14] to address the system and parameter uncertainties. In order to effectively deal with such large optimization problems in power grids hosting highly-distributed energy resources (DERs) and controllable loads, a decentralized OPF algorithm is proposed in [15], [16] relying on a dependable communication system [17]. Renewable uncertainties are also studied in stochastic economic dispatch (SED) problems in [18]–[20].

To date, centralized EMS architectures able to globally optimize EV charging schedules are either applicable to distribution systems with small-scale EV penetrations or tailored to specific EV customers with certain behaviors. EV charging management for commercial buildings with PV generation is studied in [21]. In [22], a chance-constrained control strategy is proposed for EV-integrated microgrids in which each EV is modeled as a variable making it a computationally-intensive optimization problem with large numbers of EVs. A centralized power dispatch strategy considering an aggregate model of EV fleet with certain customer behavior is approached in [23]. Regional EV charging capacity is proposed in [24] to evaluate their energy demand assuming a certain charging requirement upon arrival. EV fleets are considered as stationary storage services in [25] to reduce the transmission system operation cost. The related research mentioned above has one of the following strong assumptions on customer behavior: (i) EV customer has a certain behavior and EV demands can be precisely forecasted, (ii) EVs are assumed to be charged upon arriving home, (iii) the customers' main priority is their payments. These assumptions are contrasted to the fact that most customers require EV charging stations to charge the required EV load demand upon the EV departure, and different classes of EV customers have different preferences. They also fail to precisely characterize neither the stochasticity of the customer behavior nor the flexibility of the EV loads.

It has remained a challenge to schedule the EV charging through a global scheduling optimization problem [4]. The main obstacles to achieve a centralized charging strategy with large numbers of EVs [26] at the transmission level are: (i) perfect knowledge of the system parameters and EV customer driving profiles is not available and is hard to characterize; (ii) high computation burdens; and (iii) high communication infrastructure investment requirements. Furthermore, to our best knowledge, the system-wide correlation of EV operations with each other under plug-in and battery swapping modes and their impacts on power grid have not yet been explored in the literature. In this paper, a centralized two-stage EMS architecture is proposed to fill the knowledge gap and to be used in power systems with high proliferation of renewables and EVs. We formulate the EV scheduling problem as a global optimization problem to minimize the economic dispatch cost at the transmission level by dispatching both generators and EV load. Formulation of a global optimization problem allows the model to compute the globally optimal solution contingent on oracle forecasting. The solution of the proposed model is sub-optimal primarily due to the applied SMPC algorithm and limited observations of the EV driving profiles. However, the system uncertainties are handled by the rolling-horizon control of the SMPC algorithm and a decision making mechanism

that enables statistical estimation of the system and parameters control via two-way communications. The results indicate that the proposed two-stage EV scheduling framework can improve power system performance via a nearly-optimal solution, and at the same time, coordinates the system-level EV charging without strong assumptions of the EV customer behaviors. Furthermore, the existing communication system can be utilized with minimum required investments. The paper's main contributions are summarized as follows:

1) A two-stage EMS architecture is suggested that accounts for DER forecast uncertainties and stochastic randomness of the EV customer behaviors.

2) Effectively capturing both plug-in and battery swapping charging modes, we proposed a model that can optimize the EV charging schedules and reduce the system operation cost at the transmission level by providing a nearly-optimal solution to the global EV charging scheduling optimization problem.

3) The alternating direction method of multipliers (ADMM) is effectively employed to accelerate the computation speed of the sample-based SED problem in a DC setting and in a central station.

The rest of the paper is organized as follows. Section II presents the suggested 2-stage EMS architecture. Section III introduces the proposed first-stage optimization problem and the corresponding mathematical formulations for the SED. Section IV presents the second-stage EV charging strategies under both plug-in and battery swapping modes. Section V presents the numerical case studies and simulation results. Section VI discusses the scalability and optimality of the proposed models, followed by the conclusions in Section VII.

## II. THE PROPOSED CHANCE-CONSTRAINED EMS ARCHITECTURE

The proposed EMS architecture is illustrated in Fig. 1. We assume in this paper that both EV operation modes, plug-in or battery exchange, are viable options and customers who prefer exchanging the batteries through the BSS can subscribe in this service. The customers who charge their EVs under the plug-in mode and do not subscribe in the BSS service can still swap their depleted EV batteries with a higher price. The AMI is utilized to manage the EV energy demand by analyzing the data from smart meters connected to EVs. The EMS design in [14], [22] is modified to integrate the EVs and DERs in modern power grids. The proposed control framework is composed of two stages. The first stage is centered on a SED optimization to determine the hour-ahead dispatch target ($\Delta t_1 = 1$ h) capturing the system uncertainties. The second stage shrinks the control horizon to 5 minutes ($\Delta t_2 = 1/12$ h) and is tailored to an Optimal Power Flow (OPF) mechanism to dispatch the available resources including the controllable loads and storage units with respect to system dynamics and the first-stage targets. In particular,

1) In Stage 1, the SED is solved at time $t$ with an $L_1$-hour look-ahead rolling horizon based on the SMPC. We assume $L_1$ to be equal to 24 hours. Stochastic forecast of renewable and load profiles, estimated EV energy
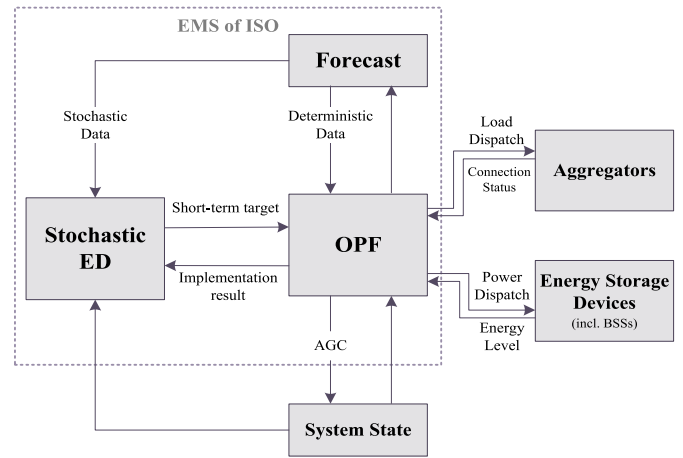


Fig. 1.   Chance-Constrained EMS Architecture: Logical View.

demand and availability (representing customer behavior), as well as system-wide battery swapping rates are effectively employed in the decision making process. If we assume an OPF look-ahead time window of $L_2$, the states of controllable loads and storage units at time step $t + L_2$ are employed as the boundary conditions in Stage 2, i.e., SED sets a short-term target for the OPF, updated hourly based on the macro system information.

2) In Stage 2, the OPF is solved with an $L_2$-hour look-ahead time window using the certainty-equivalent MPC. The charging constraint for the EVs under plug-in operation mode is updated by the aggregators through the AMI system (Section IV-A). The control mechanism of the BSS is discussed in Section IV-B. The look-ahead time window starts with $L_2/\Delta t_2$ time steps, and shrinks as time progresses to the next hour. The look-ahead time window will be changed to $L_2/\Delta t_2$ as the next hour starts. Ensuring both system and EV customer behavior constraints, the OPF engine sends the next-time-step dispatch signals to controllable loads, EV aggregators and storage units. Since the OPF engine will first try to meet the system dynamics and then to follow the SED dispatch target, its outcome may be different from the short-term plan in Stage 1. $L_2$ should be set longer than 1 hour so that the OPF does not have to follow exactly the SED dispatch signals. Deterministic forecasts are used in this stage to (i) ignore small deviations between the predicted and the realized data during a short time interval, (ii) compensate possible communication delays, and (iii) enable a fast response to system dynamics. The information and plan asymmetry in the mid-term and short-term stages are compensated periodically.

The forecast errors and dispatch delays of 5 minutes at the second-stage are addressed by the grid primary generation control and automatic generation control (AGC) mechanisms. Once the EVs' dispatch signal is acquired, it will last for 5 minutes and EVs can be regarded as constant power loads. However, if the real time communication is enabled, EVs can respond to Regulation D signals (RegD) from the independent system operators (ISOs) such as PJM market. The conditional

neutrality characteristic of the RegD allows the EVs to participate in the frequency regulation with little impact on the dispatch during system normal operating conditions. It is also worth mentioning that the stability of the power system is maintained by the traditional synchronous generators. Further research is needed to address the system stability issue under scenarios of high penetration of intermittent renewables (e.g., solar and wind) and lack of large synchronous generators.

## III. THE FIRST-STAGE SED OPTIMIZATION FORMULATION AND SOLUTION TECHNIQUE

In the first-stage SED problem, the hourly energy consumption by the swapping batteries can be forecasted as a disturbance to the optimization model. Load, wind, and solar forecasts can be also incorporated as additive uncertainties and modeled via probability distributions using weather and historical datasets. We assume the disturbance to be a sequence of independent, identically distributed random variables. Let $w_1$ be the battery swapping energy, and $w_2$ be the net load—the total renewable energy generation minus the total load. We assume that there are enough number of chargers for EVs to connect to. The availability of EVs under a plug-in operation mode depends on the total number of EVs parked, modeled as the charging upper constraint. The estimated daily EV energy consumption in the plug-in mode is modeled as the total controllable load $E_C$ during the next 24-hour interval. The first stage is implemented in a central node, sample-based SMPC method is used to solve the look-ahead SED problem in a receding-horizon manner, and distributed algorithm ADMM is used to manage the computation time.

### A. Stochastic Chance-Constrained ED Optimization Model

Monte Carlo sampling approach is employed to approximate the SED problem. A finite number of $M$ scenarios are generated, each assigned a probability of $\pi_m = 1/M$. Chance constraints are utilized so that the objective function can minimize the expected cost over all scenarios with the optimization constraints satisfied in most scenarios. Let $x(k) = \{P_{G,1}(k), \ldots, L_{c,i}(k), B_{s,n}(k)\}$ denote the state vector $x$ at time step $k$, including the real power output of conventional generating units $P_G$, controllable loads $L_c$, and the storage devices $B_s$. The input vector is denoted by $u(k) = \{\Delta P_{G,1}(k), \ldots, u_{l,i}(k), u_{c,n}(k), u_{d,n}(k)\}$ and the additive uncertainty vector is represented by $w(k) = \{w_1(k), w_2(k)\}$. Instead of the dispatch decisions following the load, we allocate both generation and load to satisfy the power balance constraints and minimize the total economic dispatch cost. The optimization problem is formulated in (1):

$$\text{minimize} \sum_{m=1}^{M} \frac{1}{M} \left[ \gamma \left( L_{c,i}^m(K+1) - E_C \right)^2 \right.$$
$$\left. + \sum_{k=1}^{K} \left( \sum_{i=1}^{n} C_i \left( P_{G,i}^m(k) \right) + 2 c_d u_{d,n}^m(k) \right) \right] \quad (1a)$$

subject to

$$x^m(k+1) = A x^m(k) + B u^m(k) + G w^m(k) \quad \forall k \ \forall m \quad (1b)$$

$$0 = C x^m(k) + D u^m(k) + E w^m(k) \qquad \forall k \ \forall m \quad (1c)$$

$$H \cdot P_{net}^m(k) \le F \qquad \forall k \ \forall m \quad (1d)$$

$$u^m(k) \in U(k) \qquad \forall k \ \forall m \quad (1e)$$

$$\mathbf{Pr}\left[ x^m(k) \in X(k), \ \forall m \right] \ge 1 - \epsilon \qquad \forall k \quad (1f)$$

where $A, B, C, D, E$, and $G$ are the state-space system matrices and fixed. $F$ is the vector of the transmission line flow limits, and $H$ is the power transfer distribution factor (PTDF) matrix. $P_{net}$ is the vector storing intermediate calculation of the net generation for buses. $X$ and $U$ are the feasible regions for the state trajectory and control inputs, respectively. The cost function (1a) consists of (i) the penalty on the deviations from daily energy consumption of the plug-in EVs, (ii) the quadratic generation cost of conventional units, and (iii) the battery degradation cost reflecting the frequent discharge of the BSS power to the grid. We assume the degradation cost for charging the EV batteries are paid by the customers and, hence, the total cost in the objective function only captures the extra cycles of the BSS. Constraint (1b) represents the state equation describing dynamics of the energy resources. Constraint (1c) enforces the power balance. Power loss is ignored in the model but can be considered by modifying the loads based on the estimate of the total system losses. Transmission line constraints are expressed in (1d). In (1e), the input variables are restricted to ramp rate limits of generating units, charging capacity of plug-in EVs and BSSs. Chance constraint (1f) ensures that the probability of scenarios in which the state variables meet the enforced limits is equal to or larger than $1 - \epsilon$. Hence, the operation constraints are considered to be satisfied in most scenarios. A few operation scenarios may violate the chance constraints. For example, when the load demand at a time is very high while the renewables output is very low, it will then call for power generation from other units. If the online generation capacity is not enough to provide the requisite power, the generation upper constraint will be violated. The system will use either generation reserve to meet the load demand or has to shed some loads.

Formulation (1) will result in a different solution in each scenario $m$ at time $t$. The average values of state variables at time $t + L_2$ are calculated, and the operating points of controllable loads and energy storage units are used as the final state targets of the second-stage OPF engine, while the initial state is considered the same in all generated scenarios. The charging state of the plug-in EVs is set to 0 so that the next 24-hours charging demand $E_C$ keeps constant. The residual between the estimated and actual power allocated to the plug-in EVs is measured and compensated at the next time step.

### B. Convex Approximations of the Chance Constraints

The chance constraint (1f) is generally a non-convex formulation and in need of a safe convex approximation to derive a computationally efficient solution. Taking the convex function $\phi(u) = (u + 1)_+$, where $(x)_+ = max\{x, 0\}$, gives the Markov chance constraint bound [27], [28]. Convex approximation of the generic $\mathbf{Pr}(f(x, w) \le 0) \ge 1 - \epsilon$ is expressed as

$$\mathbf{E}(f(x, w) + \alpha)_+ \le \alpha \epsilon \qquad (2)$$

**Algorithm 1** ADMM-Enabled SED Optimization

1: **Inputs:**
    system data and operation constraints.
2: **Initialize:**
    warm start.
    local variables $x^m \leftarrow$ warm start value.
    global variable $z \leftarrow x^{1:M}$.
    scaled dual variables $\lambda^m \leftarrow 0$.
3: **Repeat:**
4:     x-update, each processor solves the MPC problem.
5:     z-update, compute $z$ based on coupled constraints.
6:     $\lambda$-update, each processor updates scaled multipliers.
7:     check the termination criterion, break when satisfied.



Fig. 2.   EMS communication with plug-in EVs through AMI.

where $\alpha$ is a scalar. The parameter $\epsilon$ is fixed to 0.05, so a 5% violation of the probabilistic constraints is allowed in the optimization process. The convex approximation of (1f) employing the above relaxation approach is given by

$$max\big(x^m(k) - x^{max}\big)) \le TU^m \qquad \forall k \ \forall m \qquad (3a)$$

$$max\big(x^{min} - x^m(k)\big) \le TU^m \qquad \forall k \ \forall m \qquad (3b)$$

$$\frac{1}{M}\sum_{m=1}^{M}\big(TU^m + \alpha\big)_+ \le \alpha\epsilon \qquad (3c)$$

where $TU$ is also a scalar. Therefore, with the convex approximation of the chance constraint, the relaxation formulation of the SED problem remains a convex problem.

### C. Distributed Stochastic ED Optimization via ADMM

The ADMM approach is employed in this paper to speed up the computation of the chance-constrained optimization problem. The state variables in (1) are $x_i(k) \in \mathbf{R}^{n \times K}$. We gather $x$ values in all the generated scenarios and form a 3-dimensional matrix $z$ where $z_i^m(k) \in \mathbf{R}^{n \times K \times M}$. We define $\lambda$ as the scaled dual variable of the ADMM with the same dimension as $x$. The problem can be then rewritten as the global consensus problem [29] with the common global variable $z$. The steps to implement the ADMM procedure are summarized in Algorithm 1.

In step 2, a warm start is realized by solving the certainty equivalent MPC problem of the optimization formulation in (1). The suggested warm start can significantly reduce the number of ADMM iterations. In step 4, the problem (1a) to (1e) is split to a number of smaller MPC problems where scenarios can be solved in parallel. In step 5, the local variables are aggregated to consider the coupling information (1f) which is converted to convex constraints (3) and the ADMM iterations include solving small convex optimization problems. The MPC problems in x-update can be accelerated by customized solvers. The computation time of z-updates depends on the total number of samples $M$ and can be solved in only one CPU. 3-dimensional variables were converted to 2 dimensions to solve the optimization problem in this step, in order to further reduce the computation time.
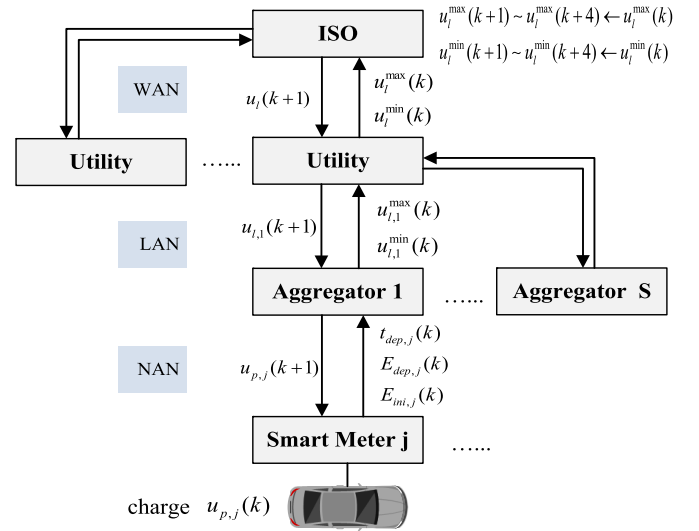
## IV. THE SECOND-STAGE EV CHARGING STRATEGY AND SIGNAL COMMUNICATION

The second-stage optimization solves a short-term deterministic DCOPF and enables a two-way communication. Here, the convex DCOPF-based optimization formulation is preferred, since DCOPF is reliable and has a lower computation burden compared to the OPF in AC setting. The DCOPF optimization followed by an AC-feasibility check can ensure that the solutions are feasible in real-world operation of transmission system. The second-stage optimization results in the total power dispatched to all generation resources and the total loads allocated to all EV aggregators at the distribution level. The total aggregated load to all EV aggregators will be proportionally distributed based on the charging capacity upper and lower limits. Distribution line limits can be considered as constraints for the charging stations. The upper bound limits of the aggregator charging constraint—i.e., based on the number of available EVs— can be enforced as the distribution line limit minus the forecasted feeder load.

Following the second-stage dispatch and utility communications with EV aggregators, the reactive power dispatch signal can be sent to charging stations and voltage magnitudes can be compensated locally, combined with regulating transformers in the distribution system. Alternatively, the voltage-reactive power mode can be activated and charging stations can facilitate maintaining the voltage at each node autonomously with lower level control. The IEEE Std. 1547-2018 also requires the DERs to provide a capacity to inject and absorb the reactive power. Hence, the proposed architecture is in line with the current operation and standardized visions, and can be applied directly to the legacy systems in practice. Note that as the proposed model can keep the distribution system active power within the distribution line thermal limits and node voltages within the desired thresholds, only the communication and power flow between the utility and plug-in EVs are modeled (Fig. 2). The EV loads are aggregated to the associated bus as additive load and OPF is run at the transmission level.

The downstream dispatch signals and the upstream estimation of the EV charging constraints are transmitted simultaneously. The EMS system and utilities communicate through the wide area network (WAN), the utilities and charging stations communicate through local area networks (LANs), and the charging stations and plug-in EVs communicate through the neighborhood area networks (NANs). Note that the LAN-level signals can be transmitted via the AMI in [3]. The NAN level required EV signal collection and direct load control implementation has been validated by the EVCS in [30]. The EV customer privacy is preserved as only the aggregated information is uploaded to the EMS (Fig. 2).

### A. Control Strategy for EVs Under Plug-in Operation Mode

A multi-agent framework is suggested to manage the EVs charging demand under the plug-in mode. The customers only need to set the EV departure time $t_{dep}$ and minimum state of charge (SOC) requirement $E_{dep}$ when they plug in their vehicles, or such information can be populated automatically using a default weekly driving profile. The aggregators receive the above information and SOC data $E_{ini}$ from the smart meters connected to each EV. Aggregators also control the EV charging energy demand at each time interval $k$. The second-stage communication and controls for EVs under plug-in mode are illustrated in Fig. 2. It details the signal and data flow among the OPF, EV aggregators and EVs in Fig. 1. The following procedure is proposed to charge the plugged-in EVs:
1) *Initialization:*
   a) Import the EV charging capacity vectors $u_l^{min}$, $u_l^{max}$ based on the EV availability.
   b) Import the system parameters and forecasts into the EMS and evaluate the first-stage charging vectors.
2) *Main Procedure:*
   At each time interval $k$, the system parameters and the EV model will be updated as follows:
   a) The EMS calculates the total power allocated to the utility $u_l(k+1)$, and the power allocated to the EV group $s$ that is managed by the corresponding aggregator, $u_{l,s}(k+1)$.
   b) The vehicle information $t_{dep}$, $E_{dep}$ and $E_{ini}$ are uploaded from the smart meters to the aggregator database, via which it calculates the charging capacity $u_{l,s}^{min}(k)$ and $u_{l,s}^{max}(k)$ of the EV group $s$.
   c) The aggregator evaluates the charging vector $u_{p,j}(k+1)$ and downloads the control variables to smart meters for EV charging in the next interval.
   d) The EMS replaces $u_l^{min}(k+1)$ to $u_l^{min}(k+4)$ with aggregated $u_l^{min}(k)$, and also $u_l^{max}(k+1)$ to $u_l^{max}(k+4)$ with the aggregated $u_l^{max}(k)$ uploaded from the aggregator database.
   e) Update the SOC of connected EV $j$ with $u_{p,j}(k)$.

In the main procedure above, step pairs (a)-(b) and (c)-(d) can run in parallel. In step (a), $u_l(k+1)$ is allocated proportionally to each EV group $s$. The ratio is actually the mean charging capacity $u_{l,s}^{min}(k-1)$ and $u_{l,s}^{max}(k-1)$ of the EV group $s$ to the mean total charging capacity $u_l^{min}(k-1)$ and $u_l^{max}(k-1)$. We limit the $u_{l,s}(k+1)$ within the range of $u_{l,s}^{min}(k)$ to $u_{l,s}^{max}(k)$

at step (c), so the implementation delay of the proposed charging strategy is 5 minutes (equal to the time-step in Stage 2). We assume that the charging capacity for a large number of EVs does not change drastically within a short time interval, thus the charging capacity at the next 20 minutes is updated with that in step (d). We assume the sliding time window of the EV aggregator is 24 hours starting from the current time interval $k_1$, and $k_{2,j}$ is the departure interval for each EV $j$ at time $t_{dep,j}$. The charging schedule for each aggregator $s$ considering the EVs' departure time and battery SOC is found in an optimization model formulated below:

$$\text{minimize} \quad \sum_j \left( \frac{E_{p,j}(k_1+1) - E_{dep,j}}{k_{2,j} - k_1} \right)^2 \tag{4a}$$

subject to

$$E_{p,j}(k+1) = E_{p,j}(k) + \Delta t \cdot \alpha_c u_{p,j}(k) \qquad \forall k \ \forall j \tag{4b}$$

$$\sum_j u_{p,j}(k_1+1) = u_{l,s}(k_1+1) \tag{4c}$$

$$E_{p,j}(k_{2,j}) \geq E_{dep,j} \qquad \forall j \tag{4d}$$

$$0 \leq E_{p,j}(k) \leq E_{cap,j} \qquad \forall k \ \forall j \tag{4e}$$

$$0 \leq u_{p,j}(k) \leq u_{p,j}^{max} \qquad \forall k \ \forall j \tag{4f}$$

The optimization model prioritizes the EV charging schedules in (4a). Constraint (4b) represents the stage functions of EV batteries. Constraint (4c) enforces the total charging capacity of the aggregator equal to the power signal sent by the utility. Constraint (4d) requires the SOC of the EVs to be higher than the customer minimum requirement upon departure. Constraints (4e) and (4f) restrict the EV battery capacity and power, respectively. The $E_{dep,j}$ is set to be 1.2 of the minimum requirement but limited to its capacity. As the EVs' charging capacity and vector are calculated by each aggregator, the problem turns into a moderate size optimization, intact, and can be parallelized. Only the aggregated EV information will be communicated between the EMS and the aggregators. When the batteries of the plug-in EVs are depleted, the customers are assumed to swap their batteries with fully charged batteries at the BSS.

It is worth mentioning that the proportional allocation of the total load $u_l(k)$ to each charging station within its limits ensures that each charging station has a certain level of flexibility. A few EV owners may prefer to minimize the total charging time instead of charging their EV batteries to the required SOC upon departure and enjoy a lower price to charge their EVs. Once the customer sets the EV charging target as to minimize the charging time, from the EV charging station perspective, the upper bound charging constraint remains the same while the lower bound charging demand increases. Through the suggested two-way communication platform, the utility will allocate the power within the charging capacity upper and lower limits to the charging station. The EVs owned by such class of customers with customized preferences will be charged during that time period based on the EV charging priority model listed in equation (4). Hence, our proposed EV

TABLE I
GENERATOR PARAMETERS OF THE 12-BUS TEST SYSTEM

| Unit $i$ | $a_i$ ($\$/MW^2$) | $b_i$ ($\$/MW$) | $c_i$ ($\$$) | $P_{G,i}^{min}$ (MW) | $P_{G,i}^{max}$ (MW) | $\Delta P_{G,i}^{min}$ (MW-h) | $\Delta P_{G,i}^{max}$ (MW-h) |
|---|---|---|---|---|---|---|---|
| $G_1$ | 0.0015 | 5.063 | 66.338 | 450 | 900 | -250 | 250 |
| $G_2$ | 0.0038 | 10.725 | 48.713 | 50 | 500 | -1200 | 1200 |
| $G_3$ | 0.0081 | 10.248 | 81.659 | 50 | 300 | -2400 | 2400 |

charging strategy does not rely on strong assumptions of customer behaviors, and can be employed to satisfy different EV customer demands simultaneously.

### B. BSS Model for EVs in Battery Exchange Mode

The BSS can be modeled as a queuing network: the EVs form an open queue and the batteries circulating in a close queue [31]. The number of batteries in the BSS will be, hence, constant. We assume that the BSS reserves enough number of fully-charged batteries for EVs to exchange as needed. We also assume that there are enough number of swapping servers and the batteries can be swapped when the EVs arrive. Then, the BSS can be regarded as an energy storage resource with the power converted to the stored energy $u_c$, the power converted to electricity $u_d$, and the energy consumption $u_s$ during each time interval based on the battery exchange rate. If $i$ denotes the number of an energy resource, the BSS energy dynamics $B_s$ can be represented as follows:

$$B_{s,i}(k+1) = B_{s,i}(k) + \Delta t \left( \alpha_c u_{c,i}(k) - (\alpha_d)^{-1} u_{d,i}(k) \right) - u_{s,i}(k) \quad (5)$$

The self-discharge of the batteries is here ignored. $u_s$ is the total energy consumption of customers who subscribe the service and those who use the plug-in charging but occasionally need the BSS service to meet the EV energy demand.

## V. NUMERICAL CASE STUDIES

A modified 12-bus test system in [32] is utilized to verify the performance of the proposed EMS architecture. As illustrated in Fig. 3, the system consists of 3 conventional generating units: one coal-fired ($G_1$) and two natural gas units ($G_2$, $G_3$), parameters of which are presented in Table I. The aggregated charging demand for EVs under the plug-in mode is modeled as a controllable load ($L_{c,4}$) and the BSS is regarded as a special energy storage resource ($B_{s,5}$). All the five resources are considered dispatchable. This test system hosts two DER units: a wind farm ($R_1$) and a photovoltaic (PV) power plant ($R_2$) with the total capacity of 200 MW and 120 MW, respectively. Hence, the total capacity of the solar and wind power is 320 MW and features nearly 16% penetration in terms of the total generation capacity. The predicted and actual data for renewable and load forecasts are taken from ERCOT in [33] and the weekly data captured in the week of December 18, 2017 in Texas is utilized in our simulations. The scale factor for wind farm, PV plant, and the load are 1/100, 1/10, and 1/32, respectively. The day-ahead forecasts are replaced by the current-day forecasts in an hour-ahead manner. A Gaussian
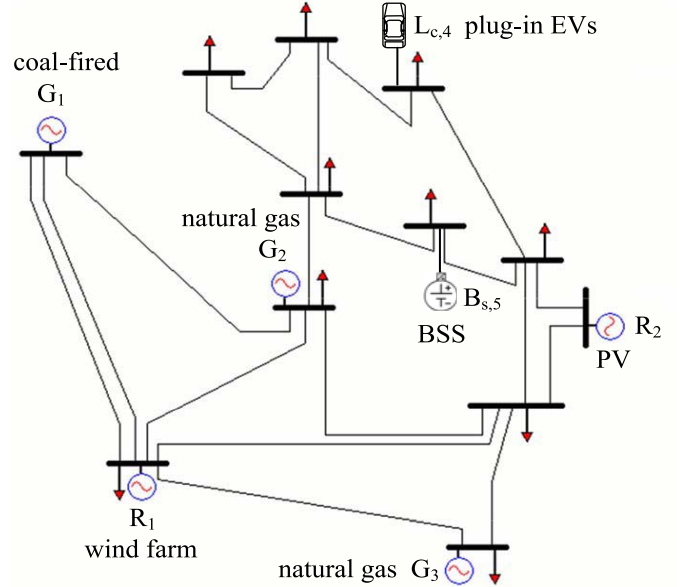


Fig. 3. The studied testbed: a modified 12-bus test system.

probability distribution truncated at $\pm 2\delta$ is utilized to represent the load and renewable forecast errors, where $\delta$ denotes the standard deviation. Uncertainty levels larger than $\pm 2\delta$ is assumed to be handled by load curtailments and generation reserves.

The target area is assumed to be hosting 100,000 EVs accounting for 30% of the total vehicles. The charging/discharging efficiencies are 90%. The EV battery capacity is 70 kWh and $c_d$ is set to 21.4 \$/MWh. There are 70,000 EVs under plug-in mode and the remaining are operated under the battery swapping mode. Driving profiles for EVs under plug-in mode were obtained from the NHTS database [34], [35]. 1000 driving profiles in Texas are randomly selected to account for the customer behaviors of plug-in EVs. The initial SOC of the EVs is uniformly distributed between 0 to 80% of the battery capacity. The charging power is set to 10.2 kW. We also assume that the customers will plug-in their EVs to charge when the parking time is longer than half an hour. Each aggregator is assumed to manage 100 to 200 connected EVs. The BSS capacity is set to 525 MWh. We reserve 20% of BSS capacity for battery swapping, so a penalty will be added when the SOC of the BSS is lower than 20%. The SOC of the BSS could not be lower than 5% in order to protect the batteries. The charge/discharge rate of the BSS is 121 MW. The estimated energy consumption of battery swapping is derived from [36] based on the EV arrival rates. The actual energy

TABLE II
SYSTEM OPERATION COSTS IN DIFFERENT TEST CASES

| TC | Total Cost ($) | Execution Time (h) |
|----|----------------|--------------------|
| 1  | 1,431,438      | 0.1                |
| 2  | 1,459,430      | 34.8               |
| 3  | 1,457,545      | 46.2               |
| 4  | 1,457,391      | 39.8               |



Fig. 4. 3-hour-ahead SOC operation targets of the BSS: The first-stage SED outcome on Friday, 22 December 2017.



Fig. 5. The charging curve and upper/lower charging constraints of the aggregated EVs under plug-in mode.

consumption of the battery swapping is randomly generated using Poisson probability distribution.

### A. Simulation Results

7 days of system operation are examined in the simulations. $L_1$ is equal to 24 hours, and $L_2$ is equal to 3 hours. We evaluate several different test cases (TC): (TC1) the base case, where the optimal solution with complete knowledge of renewables and load curves is found and the EV customers behavior exactly match that of the general estimations; (TC2) the certainty equivalent MPC, in which the uncertain parameters are substituted by the forecasts mean values; (TC3) the SMPC, in which the SED is calculated as one large optimization problem; (TC4) the SMPC, in which the SED is distributed using the ADMM method where $x$-update and $z$-update are solved using CVXGEN and SeDuMi solvers, respectively. Using CVXGEN [37], the $x$-updates can be managed very fast, even executed in series, as each MPC problem can be solved in milliseconds. All test cases are simulated with CVX optimizer in MATLAB 2017a on a Dual 8-Core 2.6GHz Intel Xeon machine.

Comparison results are summarized in Table II. The cost values found in TC2, TC3, and TC4 match the base case (TC1) as the proposed EMS architecture intelligently utilizes both the macro (system-wide) and micro (AMI-recorded) information to dispatch the available resources. The ADMM-enabled SED in TC4 runs 2 times faster than that in TC3. The approximate chance constraints in TC3 and TC4 provide conservative operating points for the plug-in EVs and the BSS. Fig. 4 demonstrates that the MPC problem in TC2 requires the BSS to operate at its lower capacity during weekly peak-load intervals, still not as conservative as that in TC3 and TC4. The difference between the operating points and the simulation results in TC3 and TC4 is primarily driven by the ADMM method which ensures an optimal convergence, even with sub-optimal solutions that may vary.

Note that the base case scenario in TC1 assumes a complete knowledge of renewable power outputs, customer load curves and battery swapping curves of BSSs. However, the availability of EVs under plug-in operation mode is modeled as the charging upper constraint, the charging lower constraint is assumed to be 0, and the aggregated EV demand is assumed to be flexible which can be scheduled during the day. Hence, the constraints and the EV demand under plug-in operation mode are the relaxation formulation to the actual EV charging optimization problem. Therefore, the simulation result in TC1 is a computationally tractable lower bound compared with the intractable 'optimal' solution for large-scale EV charging
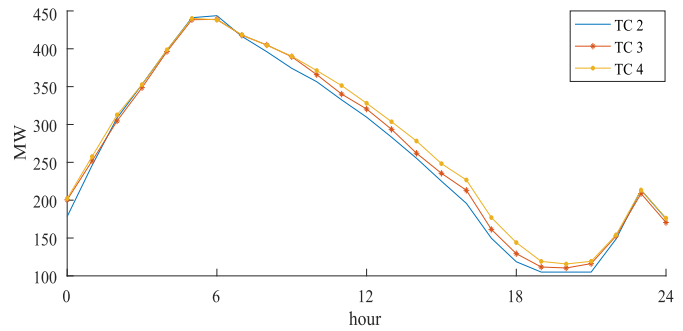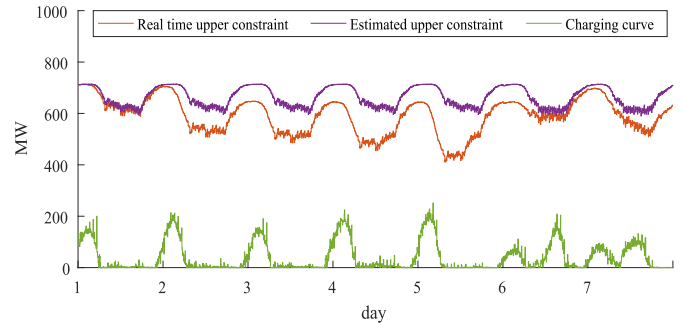
problems caused by the curse of dimensionality. The operation cost difference between TC1 and TC4 is 1.81%, so the optimality gap between the 'optimal' solution and that found in TC4 is less than 1.8%. Note that the optimality gap is primarily driven by the forecast errors.

### B. EV Dynamics and Impacts on Grid Operations

The EVs' charging schedules and the aggregated charging constraints evaluated under the plug-in mode are demonstrated in Fig. 5. The EVs parking duration less than half an hour is ignored, thus the real-time upper charging constraint is less than that estimated using the EV availability data from the NHTS dataset. It, however, revealed a small impact on the EVs' charging schedules since the maximum charging power sent from the EMS to aggregators is less than 250 MW. EVs under plug-in mode will charge mostly during the night load valley and a few charge the minimum required energy during the day-time peak hours. The real-time lower charging constraint is nearly 0 which is not included in Fig. 5.

Penetration of EVs and DERs will significantly affect the SED solutions. According to Fig. 6, the impact of EVs alone on the load profile is not significant with no obvious super off-peak EV charging hours. If both EVs and DERs are considered, the modified net load profile can be characterized as the difference between the original load plus the EV demand and the DER power generation plus the BSS discharge. Hence, the load profile will then change sharply as demonstrated in Fig. 7. The system minimizes the total operation cost which reduces the load variations. The increased noise in the load
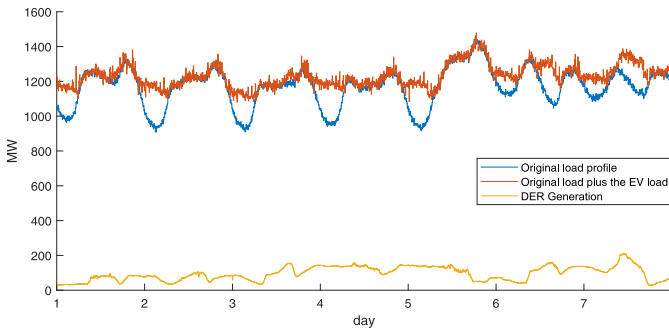
Fig. 6. Comparison of the original and the modified load profiles with 16% renewable and 30% EV penetration, when only EV load impact is considered.
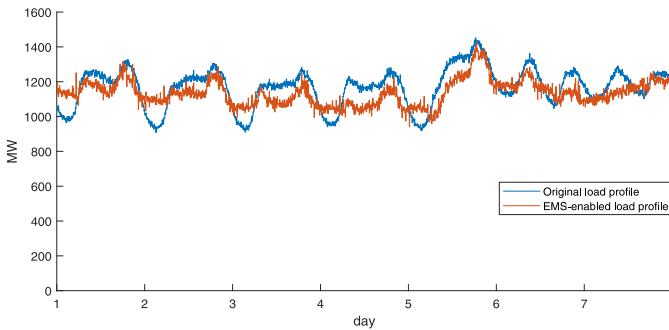


Fig. 7. Comparison of the original and the EMS-enabled load profiles with 16% renewable and 30% EV penetration.
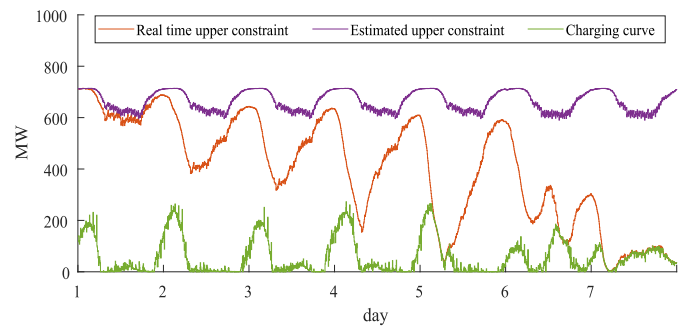


Fig. 8. The charging curve and charging constraints of the aggregated EVs with 1.5 $E_C$ in TC4.

TABLE III
COMPUTATION TIME VS. DIFFERENT NUMBER OF SAMPLES

| M | 50 | 100 | 200 | 300 | 400 | 500 |
|---|---|---|---|---|---|---|
| TC3 (s) | 108 | 252 | 712 | 1265 | 2015 | 3027 |
| TC4 (s) | 42 | 74 | 180 | 318 | 561 | 751 |
| time ratio | 2.58 | 3.39 | 3.96 | 3.98 | 3.59 | 4.03 |

### C. Solution Robustness

The estimated energy consumption of the EVs under plug-in mode in the next 24 hours may be different from the real energy demand, or in some cases depending on the weekly loading conditions and weather variations, the utility may desire to adjust the $E_C$ to increase the daily energy charged by the plug-in EVs when the next-week forecasts are available. Although the real-time upper constraint for the plug-in EVs will decrease and is different from the estimated value, the system will still stably operate within the operating limits as the OPF acquires the real-time maximum and minimum charging constraints of the plug-in EVs. The aggregated SOC of the connected EVs and the difference between the charging demand and the actual energy charged can be uploaded to the SED engine routinely, through which the SED can adjust the charging demand accordingly. Fig. 8 illustrates the charging curve with 1.5 $E_C$ in TC4 where the system is observed to be robust. We reduce 60 MW in $E_C$ when the aggregated SOC reaches its 80% capacity. But the aggregated SOC of the plug-in EVs will still reach to 99.1% at the end of the 7th day and there is 148.1 MWh unfulfilled charging demand. The $E_C$ can be then adjusted back to the original value or less at the beginning of the next week.

### D. Sensitivity Analysis and Role of Uncertain Parameters

*1) Performance of the ADMM-Enabled SED:* The execution time reported in Table II reflects the system simulation run time in 7 days and includes the time of solving hourly SED optimization, 5-minute DCOPF optimization, and dynamic simulations of the driving profiles for EV customers under plug-in mode. The number of samples $M$ in the first-stage SED problem—which was set 100 in the simulations—has a significant impact on the performance of the SED problem as the total number of variables is $269 * M$. The sample-based SMPC method is robust to any distribution of uncertainties as the suggested approach is based only on samples that are generated from the distributions, and does not rely on certain types of distributions. But the computation time increase exponentially as the number of samples increases. The sensitivity of the average computation time of the first-stage SED problem with variations in $M$ is shown in Table III. With the same samples, ADMM-enabled SED in TC4 has a better performance than the large-scale SED optimization in TC 3 and the difference in computation time can be further highlighted as $M$ increases. Deterministic sampling can be applied to keep a medium number of samples, while ensuring the SMPC convergence.

*2) Massive Penetration of EVs:* The weekly peak load is realized at 7 p.m. on Fridays as shown in Fig. 6. With 30% EV penetration in the grid, the SOC of the BSS reaches 20% of its capacity at 8 p.m., thus even if the forecast of the additive battery swapping consumption of the unsubscribed EV customers is not considered, the BSS charging to avoid the penalty of its SOC below 20% will not create a new weekly peak. However, when the EV penetration level exceeds 60% to 90%, the BSS reaches 20% of its capacity at or before 7 p.m. even with the SED approach applied. The BSS will charge during weekly peak loads to avoid the penalties and creation of a new peak. If only the EV load impact is considered, Fig. 9 shows that the new peak is 1594 MW at 7 p.m.

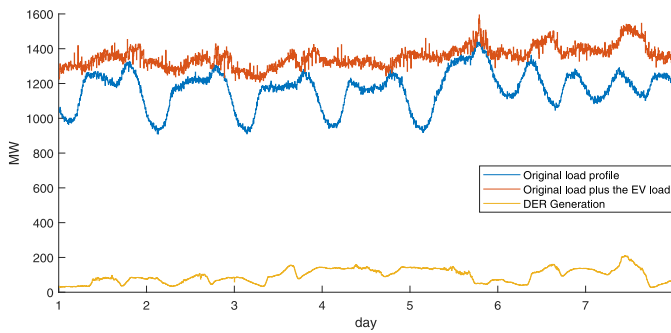profile is primarily driven by the system uncertainties and communication delays.

Fig. 9. Comparison of the original and the modified load profiles with 16% renewable and 90% EV penetration when only EV load impact is considered.
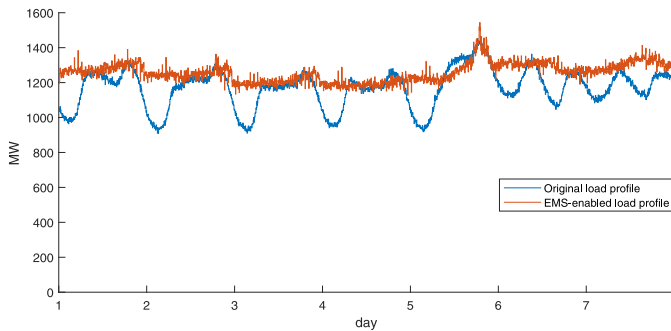


Fig. 10. Comparison of the original and the EMS-enabled load profiles with 16% renewable and 90% EV penetration.
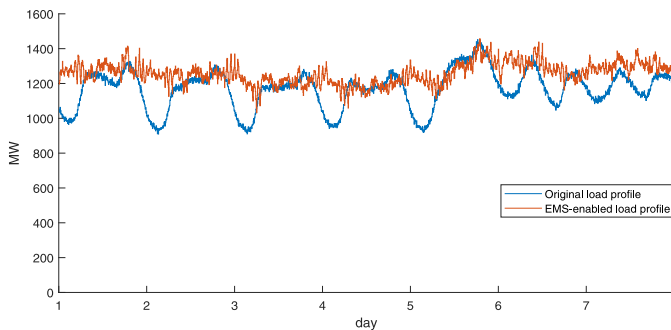


Fig. 11. Comparison of the original and the EMS-enabled load profiles with 16% renewable and 90% EV penetration, and with additive battery swapping demand forecast.

on Friday night with 90% EV penetration. If both EV load and DER generation impacts are considered, Fig. 10 shows that the new peak at that time is 1544 MW, and there will be no obvious peak and off-peak time for the EMS-enabled load profiles except the weekly peak time periods. One could realize that the additive battery swapping demand could not be ignored in cases with high EV proliferation. If the actual $u_s$ (from the simulation results with 90% EV penetration in Section V-A) is considered as the predicted $u_s$, the updated results reveal that it can avoid the simultaneous occurrence of the peak and the BSS minimum SOC by setting the BSS reaching 20% of the capacity at 8 p.m. again. The new EMS-enabled load profiles with additive battery swapping demand forecast is shown in Fig. 11.

*3) High Rate of EV Customers Subscribing the BSS Service:*
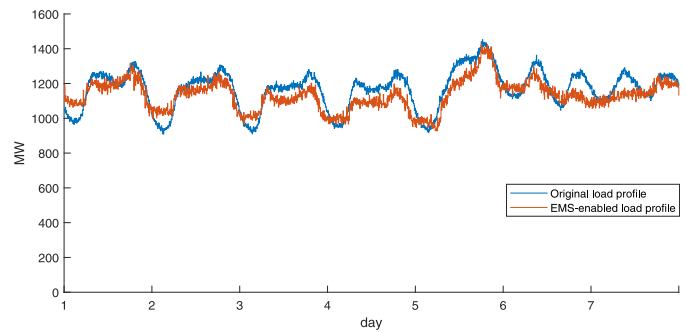We assume that a sufficient number of charging facilities for



Fig. 12. Comparison of the original and the EMS-enabled load profiles with 16% renewable and 30% EV penetration, with increased BSS customers from 30% to 70%.

the plug-in EVs exists in all scenarios and the BSS capacity does not change. With high percentage of customers subscribing the BSS service, the BSS could not fully fill the off-peak load valleys due to the capacity limits and very low battery swapping rate during the night. The BSS will charge the remaining demand during daytime off-peak hours to meet the swapping peak during 4 p.m. to 6 p.m. and avoid the minimum SOC at the peak time 7 p.m. The new EMS-enabled load profiles with 30% EV penetration and 70% subscription to the BSS service can be seen in Fig. 12, where the load variation is larger compared with that in Fig. 7. In practice, PVs can be good companions for the BSS with limited capacity. It is worth mentioning that even the BSSs are assumed to reserve a 20% capacity for battery swapping, one BSS with limited capacity may still occasionally run out of fully-charged batteries. The BSS may swap a not-fully-charged battery to the EV customer. From a system prospective, it can be regarded as a source of uncertainty for the battery swapping consumption, and will be managed in the next time interval by the EMS since it does not directly affect the power flow balance. Future research with detailed models should be devoted to the impact of BSSs capacity on the grid operation.

*4) Increasing Penetration of Renewables:* The renewable output with 16% renewable penetration and 90% EV penetration in the grid can be seen in Fig. 9, where EV load shows a characteristic of valley filling most of the time. The 12-bus test system in the case study is actually a modified IEEE 14-bus test system where no transmission line constraints are provided. Neglecting the transmission line thermal limits and when the power output of the wind and solar resources becomes 3 times larger than original, the EV load represented by the red line in Fig. 13 will present a characteristic of renewable-follower instead of valley-filler. However, the new proposed EMS engine will still try to reduce the daily variation of peak and off-peak load (see Fig. 14), as similarly observed in Fig. 10. This is because the optimization objective is to minimize the system total operation cost by dispatching both generation and EV loads.

The transmission line thermal limits can be added when congestion needs to be considered. If we assume the thermal limit for both transmission lines connected to the bus with plug-in EV load is 150 MW, Fig. 13 demonstrates that the renewable-follower characteristic of the plug-in EV load with
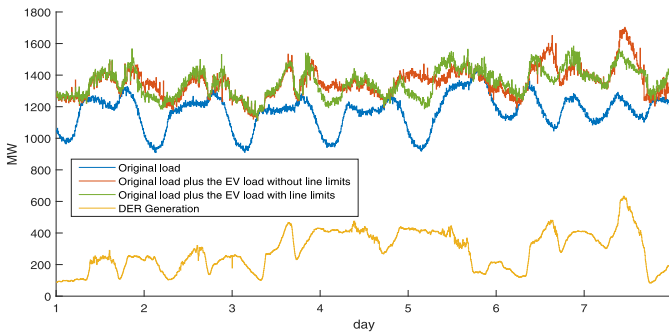
Fig. 13. Comparison of the original and the modified load profiles with 36% renewable penetration and 90% EV penetration when only EV load impact is considered.
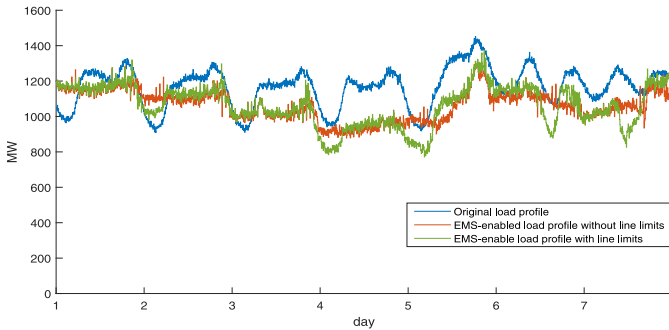


Fig. 14. Comparison of the original and the EMS-enabled load profiles with 36% renewable and 90% EV penetration.

line thermal limits is degraded compared to the case where the thermal limits are neglected, especially during the 7th day with high renewable generation. This is because the transmission line limits can affect the system capability in dispatching EV loads to minimize cost. As a result, the reduction in daily peak and off-peak load variation in EMS-enabled load profile when the transmission line limits and congestion are considered is not as obvious as the case when such limits are ignored (see Fig. 14). The operation cost in TC1 for this scenario is found $ 1,297,491, while it is observed $1,323,796 in TC4 (the optimality gap in this case is less than 2.0%).

## VI. DISCUSSION

In this section, the IEEE 118-bus test system is employed to evaluate the scalability of the proposed framework and the optimality of the suggested models. The test system specifications are taken from [38] with the following modifications: Two wind farms with rated power of 750 MW and 500 MW are placed at bus 25. One solar farm with a rated power of 650 MW is placed at bus 33. Hence, the total power capacity of the renewable sources is 1900 MW which features nearly 16% penetration in terms of the system total generation capacity. While the predicted and actual data for renewable and load forecasts are taken the same as those in Section V, scale factors of 1/16, 1/1.85, and 1/12.8 are applied for wind farms, PV plant, and the load, respectively. Truncated Gaussian probability distributions are used to represent the load and renewable forecast errors. 60 Sobol quasi-random samples are employed

### TABLE IV
### SYSTEM OPERATION COSTS IN DIFFERENT TEST CASES FOR THE IEEE 118-BUS TEST SYSTEM

| TC | Total Cost ($) | Execution Time (h) |
|----|----------------|--------------------|
| 1  | 10,847,324     | –                  |
| 2  | 10,985,851     | 35.2               |
| 3  | 10,970,532     | 44.9               |
| 4  | 10,979,744     | 44.6               |

in order to reduce the number of samples and enhance the computational efficiency of the sample-based SMPC optimization. The system is assumed to have 300,000 EVs accounting for 30% of the total vehicles. There are 210,000 EVs under plug-in mode and the remaining are operated under the battery swapping mode. The controllable load for EVs under the plug-in mode is placed at bus 115, and the BSS is placed at bus 117. Other assumptions for plug-in EVs and BSSs are the same as those presented in Section V. The same simulation configuration in Section V-A is also used except that the CVXGEN solver is not used in the x-update of TC4, as this solver is only suitable to solve small and moderate-size MPC problems rather than large MPC problems [37].

### A. Scalability

Computation comparison results of different test cases on the IEEE 118-bus test system are summarized in Table IV. Similar to those presented in Section V-A on the 12-bus test system, the cost values found in TC2, TC3, and TC4 match that of the base case scenario (TC1). However, due to the curse of dimensionality, the programming platform (MATLAB) failed to compute TC1 with a time step of 5 minutes. We, instead, used the hourly data to compute the results in TC1. Each first-stage SED problem in TC3 which is calculated as one large optimization problem can still be computed within 5 minutes since deterministic samples are used and computation time of each SED problem is ~240 seconds. The total computation time of the ADMM-enabled SED in TC4 achieves only a little faster performance than that in TC3. The degraded performance in TC4 is caused by the non-customized solver for MPC problems and also the limited available CPU cores (16 cores) to solve the x-update (which has 60 samples and results in 60 MPC problems) of ADMM method in parallel. One can conclude, from the comparison results, that the proposed chance-constrained EMS is scalable to large power grids. Note that the ADMM method to accelerate the computation speed of the first-stage sample-based SED problem in large-scale power grids requires additional CPU cores if customized MPC solvers are not used.

One needs to note that the proposed second-stage EV charging strategy is also scalable in terms of the number of EVs. This is because EV aggregators are employed to monitor and manage the charging schedules under the plug-in mode. The charging priority of EVs is calculated in parallel (simultaneously) for each EVCS during each charging period. Hence, the
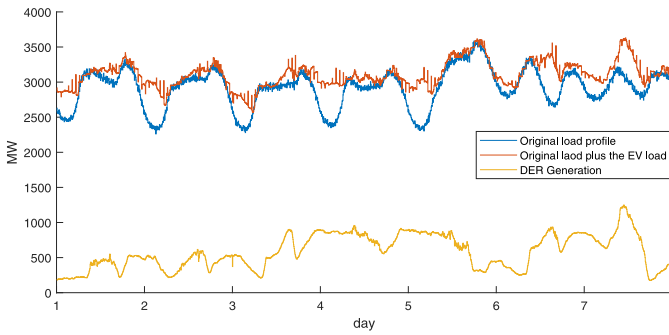
Fig. 15. Comparison of the original and the modified load profiles with 16% renewable and 30% EV penetration in the IEEE 118-bus test system when only EV load impact is considered.
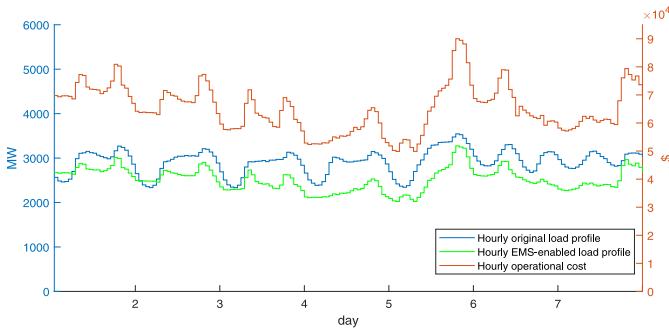


Fig. 16. Comparison of the original and the EMS-enabled hourly load profiles with 16% renewable and 30% EV penetration in the modified IEEE 118-bus test system, and the system hourly operation costs. The y axis corresponding to the EV load is located on the left, and that of the system operation cost is on the right.

computation and communication requirements for the second-stage EV scheduling problem are not burdensome, and the network size will not play a significant role.

*B. Optimality*

The penetration levels (in percentage) of renewables and EVs in this case are kept the same as in Section V-A. The total generation capacity of the IEEE 118-bus test system is, however, much higher than its original load compared with the 12-bus test system; as a result, the renewables in this case will supply more load in percentage than that in the 12-bus test system. As shown in Fig. 15, the flexibility of the EV load is utilized to either fill the super off-peak of the original load during the night, or follow the renewable output when the renewable generation is high. Similar to Fig. 7, Fig. 10, and Fig. 14, the proposed EMS engine minimizes the total operation cost and reduces the load variation (see Fig. 16).

The operation cost difference between TC4 and TC1 is evaluated 1.2% (i.e., the optimality gap of less than 1.2%). Overall and during all simulations, the optimality gap of the proposed approach is found less than or equal to 2% under different penetration levels of renewables and EVs and on different test systems. The numerical results demonstrate that the proposed method achieves a nearly-optimal solution based on the forecast accuracy available in the utility industry practices. In particular, the performance of the proposed method is mainly dependent on that of the first-stage SED

problem, i.e., the second-stage DCOPF is the deterministic optimization problem based on the first-stage calculations, and the EV charging scheduling model in equation (4) only tries to maintain the EV flexibility and prioritize the EV charging schedule. The first-stage SED problem is formulated as an SMPC problem which can achieve a nearly-optimal solution when a good forecast is available. The good forecast and system state estimation can be obtained by the proposed two-stage architecture through system level prediction and two-way communications. The optimality is maintained when using the convex relaxation of the chance-constraint optimization to solve the SMPC problem. Hence, the proposed model guarantees a nearly-optimal solution during most of the scenarios.

## VII. CONCLUSION

With the growing penetration of renewables and EVs in modern electrified power grids, advanced EMS designs are required to address the intensified system uncertainties and high-demand flexibility requirements. A two-stage chance constrained EMS architecture is proposed in this paper, where in the first stage, the system-level forecast information embedded in an stochastic MPC algorithm is utilized to optimize the short-term (next 24-hour) energy dispatch of flexible loads and storage units, while the second stage implements the dispatch signals with respect to system security and real-time requirements. The proposed EMS architecture successfully captures the real-time heterogeneous randomness in the grid and of customer behaviors—harnessing a full advantage of both macro (system-wide) and micro (AMI-captured) data—to model and dispatch the time-dependent controllable sources (e.g., EVs and storage units). Different EV charging modes and their impacts on the grid operation were extensively analyzed through which the suggested control mechanism was proven robust as it tries to meet the first-stage targets without violating the motion constraints of the individual objects. With the AMI and BSS in place, EV charging management is done via aggregators and EVs under plug-in mode were able to fill the off-peak load valleys with no large load spikes. Promising a low computational burden with an embedded distributed algorithm (ADMM) and parallel computing, the proposed EMS architecture only communicates the aggregated data and can be effectively utilized for dispatch optimization in large-scale integrated transmission and distribution models.

Future works can be directed toward: (1) utilizing other customized solvers for MPC problems with more CPU cores, facilitating the ADMM method to speed up the implementation of the first-stage SED problem in large-scale power systems with guaranteed convergence; and (2) investigating the solvability and practical algorithms to solve the chance-constrained SED with look-ahead features in AC settings.

## REFERENCES

[1] K. J. Kircher and K. M. Zhang, "Model predictive control of thermal storage for demand response," in *Proc. Amer. Control Conf. (ACC)*, Chicago, IL, USA, Jul. 2015, pp. 956–961.

[2] S. Shao, M. Pipattanasomporn, and S. Rahman, "Challenges of PHEV penetration to the residential distribution network," in *Proc. IEEE Power Energy Soc. Gen. Meeting*, Jul. 2009, pp. 1–8.

[3] B. Wang, J. A. Camacho, G. M. Pulliam, A. H. Etemadi, and P. Dehghanian, "New reward and penalty scheme for electric distribution utilities employing load-based reliability indices," *IET Gener. Transm. Distrib.*, vol. 12, no. 15, pp. 3647–3654, 2018.

[4] Y. He, B. Venkatesh, and L. Guan, "Optimal scheduling for charging and discharging of electric vehicles," *IEEE Trans. Smart Grid*, vol. 3, no. 3, pp. 1095–1105, Sep. 2012.

[5] M. Ban, M. Shahidehpour, J. Yu, and Z. Li, "A cyber-physical energy management system and optimal sizing of networked nanogrids with battery swapping stations," *IEEE Trans. Sustain. Energy*, vol. 10, no. 1, pp. 491–502, Jan. 2019.

[6] M. R. Sarker, H. Pandžić, and M. A. Ortega-Vazquez, "Optimal operation and services scheduling for an electric vehicle battery swapping station," *IEEE Trans. Power Syst.*, vol. 30, no. 2, pp. 901–910, Mar. 2015.

[7] Maigha and M. L. Crow, "Electric vehicle scheduling considering co-optimized customer and system objectives," *IEEE Trans. Sustain. Energy*, vol. 9, no. 1, pp. 410–419, Jan. 2018.

[8] S. S. Amiri, S. Jadid, and H. Saboori, "Multi-objective optimum charging management of electric vehicles through battery swapping stations," *Energy*, vol. 165, pp. 549–562, Dec. 2018.

[9] Q. Yan, B. Zhang, and M. Kezunovic, "Optimized operational cost reduction for an EV charging station integrated with battery energy storage and PV generation," *IEEE Trans. Smart Grid*, vol. 10, no. 2, pp. 2096–2106, Mar. 2019.

[10] P. Patrinos, S. Trimboli, and A. Bemporad, "Stochastic MPC for real-time market-based optimal power dispatch," in *Proc. 50th Eur.IEEE Conf. Decis. Control*, Orlando, FL, USA, Dec. 2011, pp. 7111–7116.

[11] C. E. Murillo-Sáchez, R. D. Zimmerman, C. L. Anderson, and R. J. Thomas, "Secure planning and operations of systems with stochastic sources, energy storage, and active demand," *IEEE Trans. Smart Grid*, vol. 4, no. 4, pp. 2220–2229, Dec. 2013.

[12] E. D. Anese, K. Baker, and T. Summers, "Chance-constrained AC optimal power flow for distribution systems with renewables," *IEEE Trans. Power Syst.*, vol. 32, no. 5, pp. 3427–3438, Sep. 2017.

[13] A. Mesbah, "Stochastic model predictive control: An overview and perspectives for future research," *IEEE Control Syst.*, vol. 36, no. 6, pp. 30–44, Dec. 2016.

[14] D. E. Olivares, J. D. Lara, C. A. Cañizares, and M. Kazerani, "Stochastic-predictive energy management system for isolated microgrids," *IEEE Trans. Smart Grid*, vol. 6, no. 6, pp. 2681–2693, Nov. 2015.

[15] Y. Liu, "Distributed optimization for the smart-grid," M.S. thesis, Dept. Mech. Eng., Swiss Federal Inst. Technol. Lausanne, Lausanne, Switzerland, 2015.

[16] M. Kraning, E. Chu, J. Lavaei, and S. Boyd, "Dynamic network energy management via proximal message passing," *Found. Trends Optim.*, vol. 1, no. 2, pp. 70–122, 2013.

[17] W. T. Elsayed and E. F. El-Saadany, "A fully decentralized approach for solving the economic dispatch problem," *IEEE Trans. Power Syst.*, vol. 30, no. 4, pp. 2179–2189, Jul. 2015.

[18] Y. Gu and L. Xie, "Stochastic look-ahead economic dispatch with variable generation resources," *IEEE Trans. Power Syst.*, vol. 32, no. 1, pp. 17–29, Jan. 2017.

[19] J. Li, N. Ou, G. Lin, and W. Wei, "Compressive sensing based stochastic economic dispatch with high penetration renewables," *IEEE Trans. Power Syst.*, vol. 34 ,no. 2, pp. 1438–1449, Mar. 2019. 2018.

[20] D. Hu and S. M. Ryan, "Quantifying the effect of natural gas price uncertainty on economic dispatch cost uncertainty," in *Proc. IEEE Power Energy Soc. Gen. Meeting*, Jul. 2017, pp. 1–5.

[21] Z. Liu, Q. Wu, M. Shahidehpour, C. Li, S. Huang, and W. Wei, "Transactive real-time electric vehicle charging management for commercial buildings with PV on-site generation," *IEEE Trans. Smart Grid*, vol. 10, no. 5, pp. 4939–4950, Sep. 2019.

[22] A. Ravichandran, S. Sirouspour, P. Malysz, and A. Emadi, "A chance-constraints-based control strategy for microgrids with energy storage and integrated electric vehicles," *IEEE Trans. Smart Grid*, vol. 9, no. 1, pp. 346–359, Jan. 2018.

[23] H. Zhang, Z. Hu, Z. Xu, and Y. Song, "Evaluation of achievable vehicle-to-grid capacity using aggregate PEV model," *IEEE Trans. Power Syst.*, vol. 32, no. 1, pp. 784–794, Jan. 2017.

[24] J. Zhao, J. Wang, Z. Xu, C. Wang, C. Wan, and C. Chen, "Distribution network electric vehicle hosting capacity maximization: A chargeable region optimization model," *IEEE Trans. Power Syst.*, vol. 32, no. 5, pp. 4119–4130, Sep. 2017.

[25] A. Nikoobakht, J. Aghaei, R. Khatami, E. Mahboubi-Moghaddam, and M. Parvania, "Stochastic flexible transmission operation for coordinated integration of plug-in electric vehicles and renewable energy sources," *Appl. Energy*, vol. 238, pp. 225–238, Mar. 2019.

[26] M. Latifi, A. Rastegarnia, A. Khalili, and S. Sanei, "Agent-based decentralized optimal charging strategy for plug-in electric vehicles," *IEEE Trans. Ind. Electron.*, vol. 66, no. 5, pp. 3668–3680, May 2019.

[27] S. P. Boyd. *Chance Constrained Optimization*. Accessed: Nov. 10, 2019. [Online]. Available: http://ee364a.stanford.edu/lectures/chance_constr.pdf

[28] J. Duchi. (2018). *Optimization With Uncertain Data*. [Online]. Available: http://stanford.edu/class/ee364b/lectures/robust_notes.pdf

[29] S. Boyd, N. Parikh, E. Chu, B. Peleato, and J. Eckstein, "Distributed optimization and statistical learning via the alternating direction method of multipliers," *Found. Trends® Mach. Learn.*, vol. 3, no. 1, pp. 1–122, 2011.

[30] T. Bohn, C. Cortes, and H. Glenn, "Local automatic load control for electric vehicle smart charging systems extensible via OCPP using compact submeters," in *Proc. IEEE Transport. Elect. Conf. Expo (ITEC)*, Chicago, IL, USA, Jun. 2017, pp. 724–731.

[31] B. Sun, X. Tan, and D. H. K. Tsang, "Optimal charging operation of battery swapping and charging stations with QoS guarantee," *IEEE Trans. Smart Grid*, vol. 9, no. 5, pp. 4689–4701, Sep. 2018.

[32] L. Xie and M. D. Ilic, "Model predictive economic/environmental dispatch of power systems with intermittent resources," in *Proc. IEEE Power Energy Soc. Gen. Meeting*, Calgary, AB, Canada, Jul. 2009, pp. 1–6.

[33] *ERCOT*. Accessed: Nov. 10, 2019. [Online]. Available: http://www.ercot.com/gridinfo

[34] *National Household Travel Survey*. Accessed: Nov. 10, 2019. [Online]. Available: http://nhts.ornl.gov/download.shtml

[35] X. Fang, S. Jung, and H. Zhang. *Smart Microgrid With Electric Vehicles*. Accessed: Nov. 10, 2019. [Online]. Available: https://github.com/seoho91/EV_Grid

[36] L. Cheng, Y. Chang, J. Lin, and C. Singh, "Power system reliability assessment with electric vehicle integration using battery exchange mode," *IEEE Trans. Sustain. Energy*, vol. 4, no. 4, pp. 1034–1042, Oct. 2013.

[37] J. Mattingley and S. Boyd, "CVXGEN: A code generator for embedded convex optimization," *Optim. Eng.*, vol. 12, no. 1, pp. 1–27, 2012.

[38] R. D. Zimmerman, C. E. Murillo-Sánchez, and R. J. Thomas, "MATPOWER: Steady-state operations, planning, and analysis tools for power systems research and education," *IEEE Trans. Power Syst.*, vol. 26, no. 1, pp. 12–19, Feb. 2011.

**Bo Wang** (S'15) received the B.Sc. degree in automation from Jilin University, Changchun, China, in 2013, and the M.Sc. degree in electrical power and energy from George Washington University, Washington, DC, USA, in 2015, where he is currently pursuing the Ph.D. degree with the Department of Electrical and Computer Engineering. His research interests include electric vehicles, power system optimization and control, and power system reliability.

**Payman Dehghanian** (S'11–M'17) received the B.Sc. degree in electrical engineering from the University of Tehran, Tehran, Iran, in 2009, the M.Sc. degree in electrical engineering from the Sharif University of Technology, Tehran, in 2011, and the Ph.D. degree in electrical engineering from Texas A&M University, TX, USA, in 2017. He is an Assistant Professor with the Department of Electrical and Computer Engineering, George Washington University, Washington, DC, USA. His research interests include power system protection and control, power system reliability and resiliency, asset management, and smart electricity grid applications.

**Dongbo Zhao** (S'10–M'14–SM'16) received the B.S. degree in electrical engineering from Tsinghua University, Beijing, China, in 2008, the M.S. degree in electrical engineering from Texas A&M University, College Station, TX, USA, in 2010, and the Ph.D. degree in electrical engineering from the Georgia Institute of Technology, Atlanta, GA, USA, in 2015. He is an Energy System Scientist with Argonne National Laboratory, Lemont, IL, USA. His research interests include power system control, protection, reliability analysis, transmission and distribution automation, and electric market optimization.